

MATERIALS SCIENCE

Integrating biopolymer design with physical unclonable functions for anticounterfeiting and product traceability in agriculture

Hui Sun^{1†}, Saurav Maji^{2†}, Anantha P. Chandrakasan^{2*}, Benedetto Marelli^{1*}

Smallholder farmers and manufacturers in the Agri-Food sector face substantial challenges because of increasing circulation of counterfeit products (e.g., seeds), for which current countermeasures are implemented mainly at the secondary packaging level, and are generally vulnerable because of limited security guarantees. Here, by integrating biopolymer design with physical unclonable functions (PUFs), we propose a cryptographic protocol for seed authentication using biodegradable and miniaturized PUF tags made of silk microparticles. By simply drop casting a mixture of variant silk microparticles on a seed surface, tamper-evident PUF tags can be seamlessly fabricated on a variety of seeds, where the unclonability comes from the stochastic assembly of spectrally and visually distinct silk microparticles in the tag. Unique, reproducible, and unpredictable PUF codes are generated from both Raman mapping and microscopy imaging of the silk tags. Together, the proposed technology offers a highly secure solution for anticounterfeiting and product traceability in agriculture.

INTRODUCTION

Counterfeiting has been a global, long-lasting, and unsolved issue that permeates virtually every field of our society from the luxury goods industry to pharmaceuticals. Over the years, various anti-counterfeiting strategies including holography (1, 2), watermarks (3, 4), barcodes (5, 6), quick response codes (7, 8), and radio frequency identification (RFID) tags (9, 10) have been developed, offering competitive countermeasures against growing fraudulent practices worldwide. Many of these anticounterfeiting technologies, however, are based on deterministic encoding mechanism that has inherent vulnerability to various cloning attacks. Motivated by the need to address these security vulnerabilities, the idea of physical unclonable function (PUF) was proposed (11–14), which refers to a physical object that uses its intrinsically random variations to provide a unique and unpredictable output (response) under an external stimulus (challenge). The responses of PUFs rely on their underlying physical characteristics that have stochastic and uncontrollable features introduced during manufacturing. The fact that exact control over the manufacturing process is infeasible makes it extremely difficult if not impossible to duplicate a PUF device. Because of these merits, silicon-based PUFs have been traditionally designed and widely used in integrated circuits for authentication applications (15). More recently, nonsilicon PUFs made from taggants exhibiting unique physicochemical properties (e.g., polymers, liquid crystals, fluorophore-dyed particles, and light-scattering fibers) were also proposed, which have gained increasing popularity as anticounterfeiting labels for applications such as on-dose authentication of medicines (16–18).

Despite multiple demonstrations of integrating material-based nonsilicon PUFs in anticounterfeiting designs for high-end

commodities (e.g., luxury articles and medicines) (16–20), much less attention has been given to counterfeiting and product traceability issues in agriculture. Taking the seed business for example, there has been a continuing increase in illegal seed practices, including counterfeit seeds, fraudulent labeling, trademark infringements, intellectual property infringements, regulatory offenses, and thefts of proprietary material (21). The increasing circulation of counterfeit seeds has posed a tremendous threat to both manufacturers and smallholder farmers. This is particularly true in the African continent, where it has been estimated that financial losses accounting for circa 350 million USD negatively affect a seed market valued at circa 500 million USD annually (22). As counterfeit seeds are usually associated with low germination rates and vigor, their usage in the field substantially impairs the overall capacity of global food production. According to a 2017 World Bank report (23), in some African countries, up to 50% of crop seeds sold to farmers are illegal or counterfeit, which is a major contributor to the chronic problem of farmers achieving crop yields far below the potential harvest of their lands. For example, the actual yield per hectare in a typical sub-Saharan farm is 1.5 tons for maize, 0.8 tons for legumes, and 2.1 tons for rice, as compared to a potential yield of 8, 3, and 6.5 tons, respectively (24). Current efforts to combat counterfeit seeds are implemented mainly at the secondary packaging level (25), including the use of tamper-proof packages, coin-scratch labels that are verified by end users via mobile authentication (e.g., short message service), barcodes that can be scanned at each stage of the supply chain, and RFID tags affixed to the packages. As such packages can be easily duplicated to contain fake seeds and individual seeds can also be sold without secondary packaging, these improved seed packaging approaches generally have limited security guarantees. In addition, emerging strategies that are being actively pursued to tackle counterfeits in Agri-Food systems include the use of digital images containing hidden information that are not visible to the naked eye, holograms, fluorescent dyes or luminescent pigments printed in patches on a product to create a unique signature, and taggants that have uniquely encoded microscopic features (22, 26). Although these measures

Copyright © 2023 The Authors, some rights reserved; exclusive licensee American Association for the Advancement of Science. No claim to original U.S. Government Works. Distributed under a Creative Commons Attribution NonCommercial License 4.0 (CC BY-NC).

¹Department of Civil and Environmental Engineering, Massachusetts Institute of Technology, Cambridge, MA 02139, USA. ²Department of Electrical Engineering and Computer Science, Massachusetts Institute of Technology, Cambridge, MA 02139, USA.

[†]These authors contributed equally to this work.

*Corresponding author. Email: anantha@mit.edu (A.P.C.); bmarelli@mit.edu (B.M.)

have a positive impact on anticounterfeiting in agriculture, the issues of fraudulence and insufficient product traceability remain far from being solved. In particular, a higher-level protection of authentic agricultural products from counterfeits would require higher security levels associated with the anticounterfeiting measures—an area where PUFs excel at. To the best of our knowledge, however, PUF-based solutions have not yet been explored in the Agri-Food domain. Moreover, as agricultural products such as seeds are sold in large volumes and at low profit margins, their anticounterfeiting measures require facile and low-cost implementation at scale, thus limiting the use of costly raw materials and sophisticated micro-/nanofabrication techniques involved in many of the PUF-based anticounterfeiting solutions provided so far (16, 19, 20). Besides, given that anticounterfeiting devices applied to agricultural products will inevitably end up in the environment or might be ingested during food consumption, the materials used to make those devices should ideally be biodegradable, nontoxic, and even edible. In this respect, naturally derived biopolymers like silk fibroin from *Bombyx mori* cocoons represent a promising candidate, especially given its Generally Regarded as Safe (GRAS) status for human consumption issued by the U.S. Food and Drug Administration (FDA) (27, 28).

Here, we propose a cryptographic protocol for seed authentication using biodegradable and miniaturized PUF tags made of silk microparticles (MPs) that can be directly applied on the surface of a variety of seeds. The silk MPs were first engineered to have distinct molecular fingerprints through templated crystallization and water annealing. By simply drop casting a mixture of spectrally distinct silk MPs on a seed, a PUF tag composed of stochastically assembled silk MPs seamlessly formed on the seed surface upon water evaporation, which can then be read by a Raman spectrometer to generate a PUF code. A further modification of the silk MP-based PUF was achieved by the addition of colored salts (e.g., FeCl_3) in the silk MPs suspension to allow for silk-inorganics coassembly during water evaporation, resulting in formation of random and distinct visual patterns that can be captured by a pocket microscope and processed through a similar digitization protocol. The PUF codes obtained were verified to be unique, reproducible, and unpredictable by evaluating their Hamming distances (HDs) and statistical randomness. Together, by leveraging biopolymer design with PUFs, we demonstrate the capability to establish unclonable authentication features at the individual seed level, with the requirement of a minimal amount of materials (less than 50 μg of silk per seed) and the use of easily scalable manufacturing techniques.

RESULTS

Engineering variant silk MPs for fabrication of tamper-evident tags on seeds

To obtain spectrally distinct silk MPs, we took advantage of the polymorphism of silk fibroin, which refers to its ability to assume different secondary, tertiary, and quaternary structures achieved by controlling the protein folding and assembly pathways. Here, bottom-up directed assembly and rapidly scalable top-down manufacturing were integrated to fabricate silk MPs of four different polymorphs. First, spray drying was used to generate silk MPs of sizes 2 to 20 μm (Fig. 1A and fig. S1A) (29), followed by water annealing of those particles to induce formation of ordered molecular structures and render them water insoluble (30). The choice of the

spray drying technique was based on its high efficiency in producing grams of protein powders per hour and its wide use in the industry (31). Exposing the spray-dried silk MPs to water vapor for a prolonged time (i.e., water annealing of the amorphous silk MPs) then allows the random coil fibroin chains to slowly fold into water stable type II β -turn structures (30). To obtain the other three silk polymorphs, we used a recently developed technique named templated crystallization, where highly ordered peptide nanoassemblies were used to guide the folding and assembly of amorphous silk molecules into ordered structures that resemble that of the peptide (32). This is achieved through fibroin chain reconfiguration after binding to the peptide seeds, which then template assembly of the folded fibroin chains into higher-order structures. On the basis of our previous experience in silk protein design, we selected three peptides capable of templating silk into distinct polymorphs (Fig. 1B): (i) GCGAGAGCGAGA [noted as $(\text{GCGAGA})_2$ thereafter for brevity], (ii) GAGAGSGAAS, and (iii) a coiled-coil peptide of sequence ALKAQSEEEAASARANAA-TAATQSALEG derived from the silk fibroin AmelF3 of European honeybee *Apis mellifera* (33). For simplicity, this peptide is noted as honeybee silk peptide (HBSP) thereafter. The first two peptides [$(\text{GCGAGA})_2$ and GAGAGSGAAS] self-assemble into short nanowhiskers of sizes around 200 nm by 20 nm by 4 nm (fig. S2A) and of highly ordered β sheet structures, but the molecular arrangements and packing of individual peptide chains are different as characterized by wide-angle x-ray scattering (WAXS) and Raman spectroscopy (fig. S2, B and C). HBSP also forms supramolecular nanoassemblies in water, which have a less regularly defined morphology and a combination of β sheet and α helix secondary structures (fig. S2). The templated crystallization process starts with mixing each of the three peptides with silk fibroin, after which a gradual increase in solution turbidity was observed, indicating the formation of silk-peptide nanocomplexes and their growth to micrometer sizes. After letting each solution age until the templated crystallization process reaches equilibrium, we freeze-dried the solution to obtain powders of crystallized silk. The lyophilized silk powders were then ground to finer sizes using a mortar and pestle, with the final silk particles showing a polygonal shape and ranging in size from 1 to 30 μm (Fig. 1B and fig. S1, B to D).

Raman characterization shows distinct spectral fingerprints of the four silk MPs obtained by water annealing and templated crystallization (Fig. 1C), due to differences in the underlying silk polymorphs. For example, a band at around 880 cm^{-1} [which relates to the presence of β sheets adopted by poly-(alanyl)glycine sequences (34)] is present in the Raman spectra of silk MPs #2 to 4, but absent in that of silk MPs #1, due to the lack of antiparallel β -pleated sheets in water-annealed silk (30). In addition, a band at around 1103 cm^{-1} , characteristic of type II β turns (35), is present in the spectrum of silk MPs #1 but absent in those of silk MPs #2 to 4. The intensity ratio of the tyrosine Fermi doublet at 830 and 850 cm^{-1} (which serves as a spectral marker of the environment of the phenoxyl groups and the strength of hydrogen bonds involving tyrosine residues) is also different among the four silk MPs, which is associated with different folding patterns of the fibroin chains resulting from different templating agents (36). Notable spectral differences are also evident in the amide III region (1200 to 1350 cm^{-1}) of the four silk MPs, including (i) a major band shift from around 1240 cm^{-1} in silk MPs #1 to around 1228 cm^{-1} in silk MPs #2 to 4, (ii) changes in band width at half height with sharper peaks

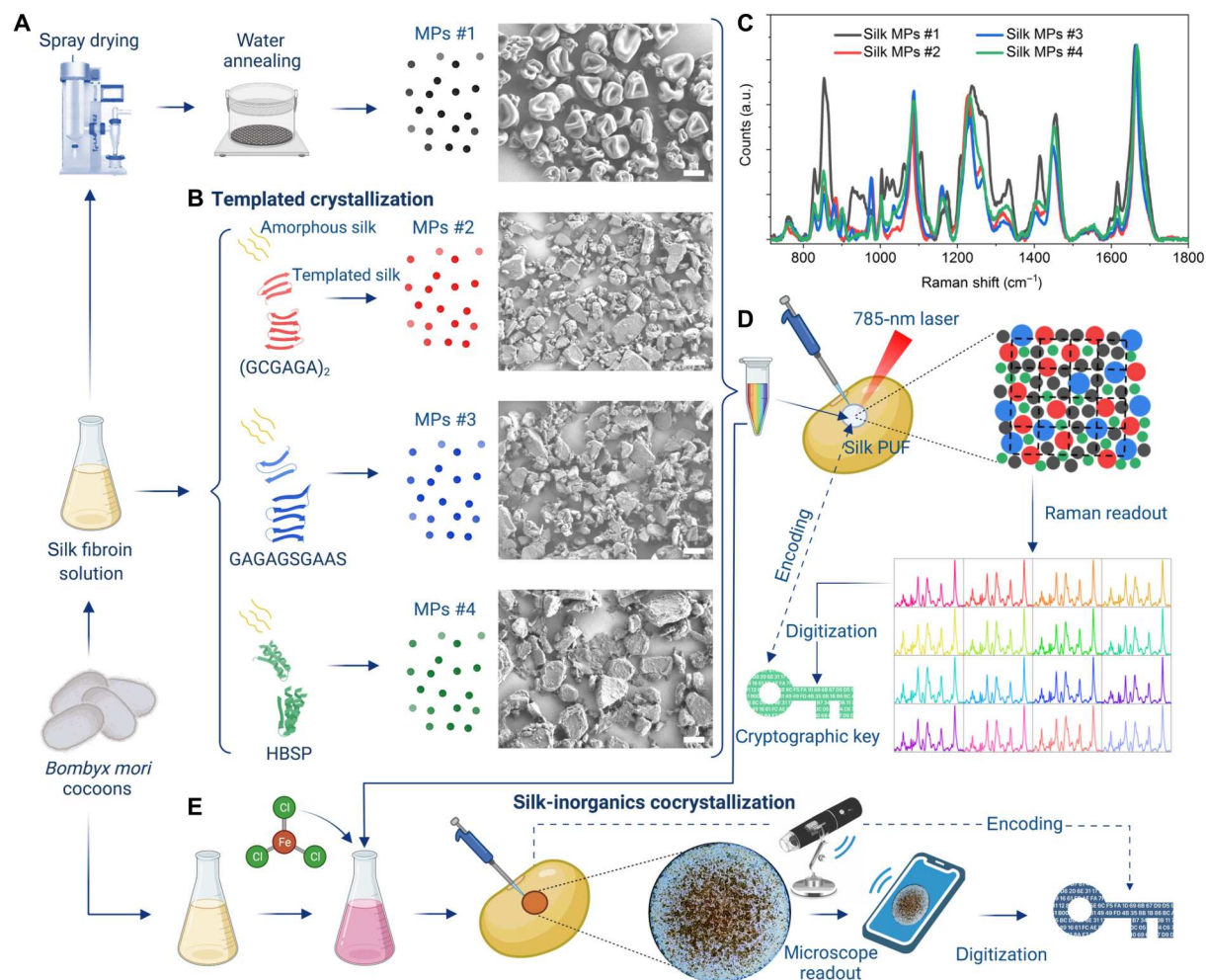


Fig. 1. Engineering spectrally and visually distinct silk MPs for fabrication of conformable tags on seeds. (A) Silk MPs #1 were spray-dried from a regenerated silk fibroin solution, followed by water annealing of the particles to render them water insoluble. Scale bar, 10 μm . (B) Silk MPs #2 to 4 were fabricated through templated crystallization of amorphous silk on three different peptide seeds. Scale bars, 10 μm . (C) The four silk MPs of different polymorphs show distinct Raman spectra. a.u., arbitrary units. (D) Schematic of the fabrication of a spectral PUF tag through drop casting a mixture of spectrally distinct silk MPs, which provides a Raman readout that is then digitized to a cryptographic key. (E) Schematic of the fabrication of a visual PUF tag made from a suspension of silk MPs doped with FeCl_3 , which is captured by a pocket microscope to provide an image readout as the input for PUF code generation.

corresponding to higher silk crystallinity (i.e., β sheet contents), and (iii) appearance and absence of bands at 1210, 1260, 1265, and 1332 cm^{-1} in silk MPs of different polymorphs. These distinctive peak features serve as the basis for digitization of the Raman readout from our silk MP-based PUF tags.

By simply drop casting a suspension containing all four silk MPs [at 0.7 weight % (wt %)] and amorphous silk molecules (at 0.3 wt %) on a seed, a white tag composed of randomly distributed and spectrally distinct silk MPs can seamlessly form on the seed surface after water evaporation. Raman mapping of a selected area in that silk tag was then performed, generating a matrix of Raman spectra followed by its digitization to a binary PUF code (Fig. 1D). We refer to this silk tag as a spectral PUF hereafter. Another variation of the silk MP-based PUF was achieved by the addition of colored salts (50 mM FeCl_3) in the silk MPs suspension to allow for silk-inorganics cocrystallization during water evaporation, resulting in the formation of random and distinct visual patterns that can be captured by

an inexpensive pocket microscope connected with a smartphone and processed through a similar digitization protocol (Fig. 1E). The choice of FeCl_3 here was based on iron being one of the essential micronutrients for plants. Given that the typical range of iron concentration in cultivated soils is 20 to 40 g/kg, our silk tags containing 28 μg of iron per tag add little disturbance to the Fe dynamics in soil ecosystems (37). More detailed analysis on the amount of exogenous iron introduced to the soil through our silk-Fe seed tags can be found in the Supplementary Materials. We refer to this silk tag as a visual PUF hereafter.

With this simple drop casting method, we were able to conformably and seamlessly fabricate silk MP-based tags on a variety of seeds (Fig. 2, A and B), such as tulip (*Tulipa gesneriana*) bulbs, corn (*Zea mays*), zucchini (*Cucurbita pepo*), apple (*Malus domestica*), eggplant (*Solanum melongena*), and bush bean (*Phaseolus vulgaris*) seeds. This demonstrates the broad applicability of our silk tags on a diverse range of seeds that have vastly different sizes,

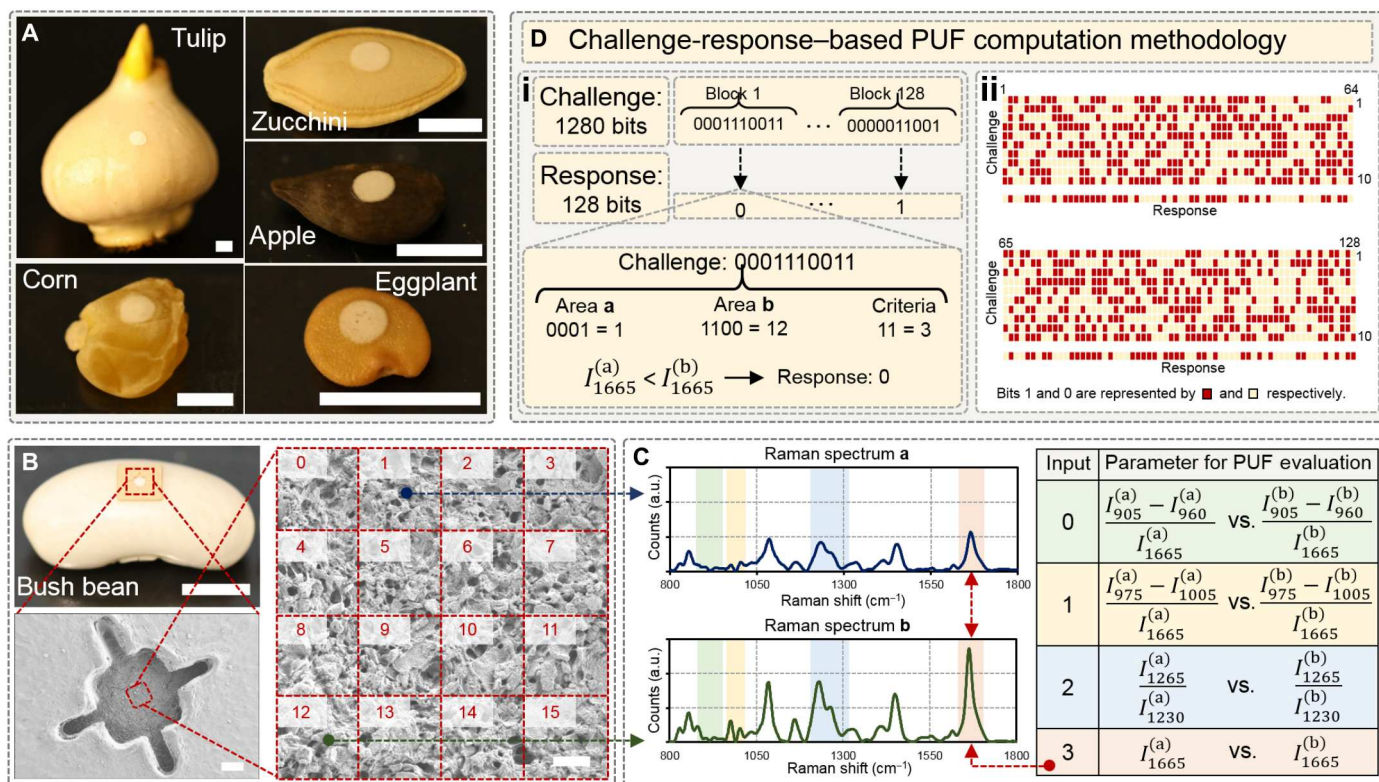


Fig. 2. PUF code extraction from the silk MP-based spectral tags. (A) Photographs of silk MP-based spectral tags assembled on tulip bulbs, corn, zucchini, apple, and eggplant seeds. Scale bars, 5 mm. (B) An adhesive mask with a cross-shaped window was applied to the silk tag assembled on a bush bean seed, to ensure Raman mapping of a fixed area within the silk tag across different measurements. Scale bar, 5 mm. SEM characterization of the silk tag showing stochastic distribution of silk MPs in the tag. A central area of 90 μm by 90 μm of the silk tag was selected for Raman mapping, and a mapping resolution of 4×4 was used throughout this study, generating 16 Raman spectra (numbered from 0 to 15) arranged in 4 rows and 4 columns. Scale bars, 200 μm (bottom left) and 10 μm (right). (C) Comparison of two Raman spectra (#1 and #12) using peak intensities at several Raman shifts—(#0) 905 and 960 cm^{-1} (α -helical peaks), (#1) 975 and 1005 cm^{-1} (breathing modes of benzene rings), (#2) 1230 and 1265 cm^{-1} (amide III peaks), and (#3) 1665 cm^{-1} (amide I peak). (D) Illustration of the challenge-response protocol for spectral PUFs: (i) The challenge comprises 1280 bits, which is organized in 128 blocks with each block being a 10-bit binary code. The response comprises 128 bits, where each response bit is obtained by comparing two Raman spectra using one of the four parameters given in (C), as indicated by the corresponding challenge block. (ii) An example PUF code of 128-bit computed from a randomly generated challenge of 1280 bit.

shapes, colors, and surface textures. Besides, the resulting silk tags are resistant to normal damaging forces such as wiping with a tablecloth and those generated during transportation (e.g., friction between seeds as well as between seeds and containers/packages). The tight and conformable bonding between our silk tag and the seed coat is attributed to the presence of amorphous silk molecules acting as an adhesive matrix that holds the silk MPs together and forms a seamless interface with the seed coat (38). Moreover, the silk MP-based tag loses its integrity as soon as it is removed from the underlying seed, making it tamper-evident. This also ensures that each silk tag only works with the seed it has assembled on, and it cannot be removed and applied on any other seed.

PUF code extraction from the silk MP-based tags on seeds

For spectral PUFs, a mask with a cross-shaped window was applied to the silk tags to facilitate mapping of the same area and to enable reproducible seed authentication at each stage of the supply chain (Fig. 2B). With the four arms of the cross, the center of the exposed silk area can be reproducibly located [denoted as (0, 0) for simplicity], thereby ensuring Raman data collection on the same area of the silk tag. Typically, a 90 \times 90 μm^2 area centered at (0, 0) was selected

for Raman mapping and a mapping resolution of 4×4 was used throughout this study. This generates 16 Raman spectra (numbered from 0 to 15) arranged in 4 rows and 4 columns (Fig. 2B). A PUF code can be generated from these 16 Raman spectra by selecting two spectra *a* and *b* and then comparing them using one of the following four parameters: (#0) $\frac{I_{905} - I_{960}}{I_{1665}}$, (#1) $\frac{I_{975} - I_{1005}}{I_{1665}}$, (#2) $\frac{I_{1265}}{I_{1230}}$, and (#3) I_{1665} , where *I* represents Raman peak intensity, and the subscript corresponds to Raman peak position in cm^{-1} (Fig. 2C). Selection of these four parameters was based on identification of the most notable variations in Raman peak features across different areas of the silk MPs tag, as previously discussed. More detailed explanation on their associated vibrational modes of molecules can also be found in the Supplementary Materials. During each comparison, if the chosen parameter of spectrum *a* is larger than that of spectrum *b*, the response generated is 1; otherwise, it is 0. As for which two of the 16 Raman spectra are to be compared and which parameter is used for comparing the two spectra, this is determined by a 1280-bit challenge [Fig. 2D(i)]. The 1280-bit challenge is composed of 128 blocks with each block being a 10-bit binary code. Taking one challenge block—0001110011, for example [Fig. 2D(i)], the first two groups of four digits (i.e., 0001 and 1100) indicate the indexes of

the two Raman spectra to be compared (i.e., 1 and 12 in decimal numbers), and the last two digits (i.e., 11) indicate the index of the parameter used to compare the two Raman spectra (i.e., parameter #3). In this case, because $I_{1665}^{(a)} < I_{1665}^{(b)}$, the response generated for this challenge block is 0. Because each challenge block generates a response of 1 bit, a 1280-bit challenge of 128 blocks then generates a response of 128 bits as the final PUF code for a spectral tag [Fig. 2D(ii)]. On the basis of this challenge-response protocol, the PUF code generated depends not only on the physical properties of the silk tags (i.e., the distribution of spectrally distinct silk MPs within the tag) but also on the challenge applied to the Raman readout. It is noted that although there are a total of $(16 \times 15/2) \times 4 = 480$ pairs of unique comparison that can be made for 16 spectra and 4 parameters, one does not have to go through every comparison for the Raman readout of each tag. The number of challenge blocks mainly depends on the desired length of PUF response (i.e., the encoding capability of PUFs) and can be chosen to be any integer in the range of 1 to 480 based on customer needs. Considering that an encoding capability of 2^{128} is sufficient for most authentication applications and for a proof-of-concept demonstration, here, we chose the PUF challenge to be composed of 128 blocks generating a PUF response of 128 bits.

For visual PUFs [Fig. 3A(i)], the PUF codes were extracted from the magnified images of silk-iron tags captured using a pocket

microscope [Fig. 3A(ii)]. Before using them for PUF computation, several image processing steps were applied to the raw microscope images (39), to standardize all images and compensate for image-to-image variations in orientation, magnification, brightness, and contrast. Therefore, no prealignment of the silk-iron tags to the microscope camera is required. A detailed description of the PUF image processing protocol as well as its robustness against variations brought by different imagers and different types of seeds can be found in the Supplementary Materials. Briefly, the silk-iron tag was first isolated using a standard edge detection algorithm and converted to a fixed-size image of 400×400 pixels [Fig. 3A(iii)] through Homography Transform—a mathematical operation that maps an image captured in one plane to a different plane (40). Because the tag image is influenced by the lighting conditions (luminance), which may vary from measurement to measurement, we extracted only the intrinsic color information of the tag image using a luminance reduction technique [Fig. 3A(iv)]. We then applied a histogram equalization-based contrast enhancement technique to increase the separation between lighter and darker regions and obtained a contrast-enhanced RGB (Red Green Blue) image of 400×400 pixels [Fig. 3A(v)]. This RGB image was then converted to a grayscale image [Fig. 3A(vi)], followed by selecting its central region of 280×280 pixels and partitioning it into $8 \times 8 = 64$ areas [Fig. 3A(vii)]. Last, the mean intensities (i.e., shades of gray) of each

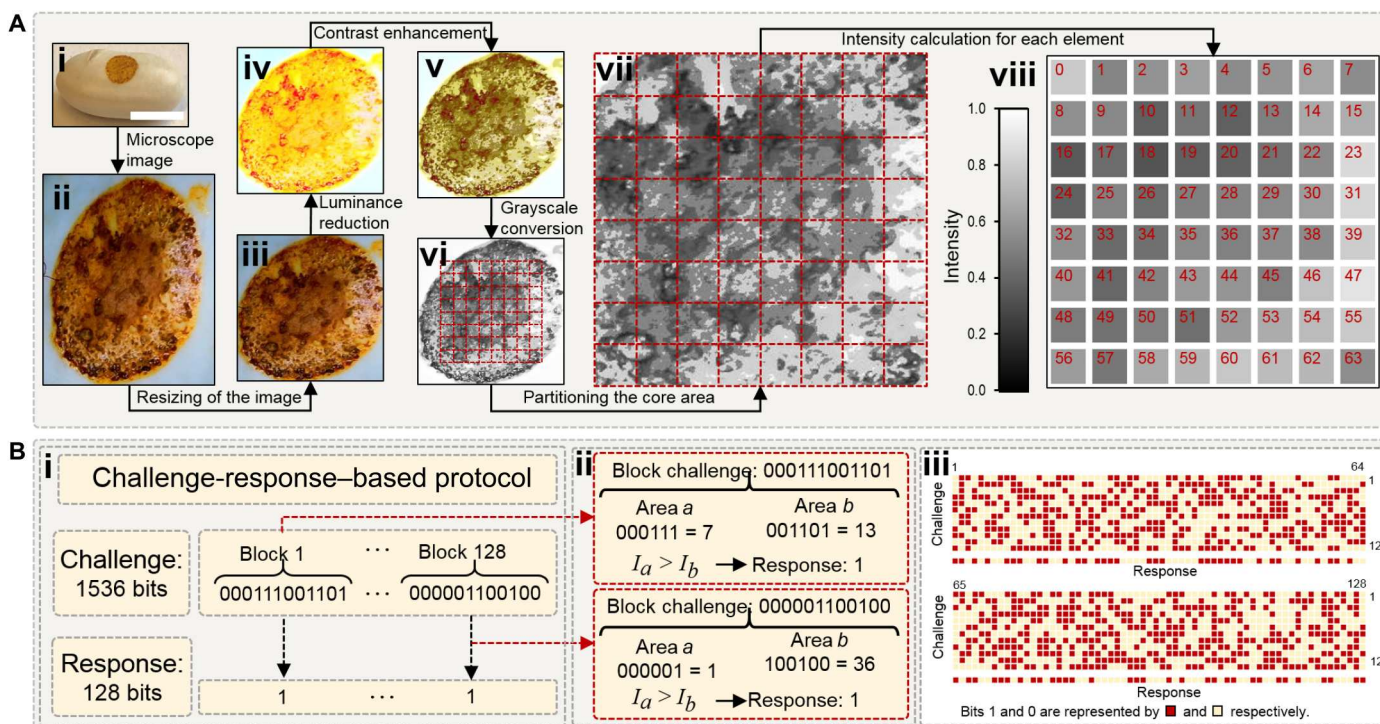


Fig. 3. PUF code extraction from the silk MP-based visual tags. (A) Processing of the silk-iron tag image to be used for PUF computation: (i) Photograph of a silk-iron tag assembled on a bush bean seed. Scale bar, 5 mm. (ii) Raw image of the silk-iron tag in (i) captured by a pocket microscope. (iii) Resized tag image of 400×400 pixels generated from the raw image in (ii). (iv) Luminance-compensated tag image containing only the intrinsic color information. (v) Contrast-enhanced tag image by applying histogram equalization to the image in (iv). (vi) Grayscale image converted from the RGB image in (v). (vii) Core region of the grayscale tag image partitioned into $8 \times 8 = 64$ areas. (viii) An 8×8 array showing the averaged intensities (i.e. shades of gray) of each area in (vii). (B) Illustration of the challenge-response protocol for visual PUFs: (i) The challenge comprises 1536 bits, which is organized in 128 blocks with each block being a 12-bit binary code. The response comprises 128 bits, where each response bit is obtained from its corresponding challenge block. (ii) Computation of PUF responses by comparing the intensities of two areas whose indexes are indicated by the given challenges. (iii) An example PUF code of 128-bit computed from a randomly generated challenge of 1536-bit.

area were calculated and represented as an 8×8 array numbered from 0 to 63 [Fig. 3A(viii)]. This intensity array was the input to the visual PUF challenge-response protocol, which is described in Fig. 3B. The PUF challenge comprises 1536 bits (organized in 128 blocks of 12 bits each), while the response comprises 128 bits, where each response bit is obtained from its corresponding challenge block [Fig. 3B(i)]. Computation of the PUF responses involves comparing the intensities of two areas a and b (denoted as I_a and I_b) selected from the 8×8 array [Fig. 3B(ii)]. If $I_a > I_b$, the PUF response generated is 1; otherwise, it is 0. The indexes of the two areas to be compared are determined by the two components of 6 bits in each challenge block. Taking the first challenge block—000111001101 for example, the first 6 bits (i.e., 000111) indicates the index of area a (which is 7 in decimal number) and the successive 6 bits (i.e., 001101) indicates the index of area b (which is 13 in decimal number). Since $I_a = I_7 > I_b = I_{13}$, the first PUF response for the first challenge block is 1. Similarly, to generate the 128th PUF response for the 128th challenge block—000001100100, I_1 and I_{36} were compared. Since $I_1 > I_{36}$, the 128th PUF response is also 1. Following this challenge-response protocol, a complete PUF response of 128 bits was calculated from a randomly generated challenge of 1536 bits for visual tags [Fig. 3B(iii)]. The number of challenge blocks in this case can be chosen to be any integer in the range of 1 to 2016 based on customer needs.

Performance of silk MP-based PUFs

To ensure practical applicability of our silk MP-based tags for PUF-based authentication, it is important to analyze their PUF codes using relevant metrics—bit uniformity, uniqueness, repeatability, and randomness (16, 41). Accordingly, PUF codes from 30 spectral tags (Fig. 4A) and 30 visual tags (Fig. 4B) were repeatedly generated under the same challenge and statistically analyzed. Corresponding to each tag, its PUF codes are displayed in two rows with the top and bottom row representing the PUF code obtained from the first (original) and second (repeated) measurement.

Bit uniformity is evaluated to verify that the PUF code is not biased toward either bit 0 or 1. Mathematically, bit uniformity is defined as the probability of observing the digit 1 in a binary code P

$$\text{Bit uniformity}(P) = \frac{1}{L} \sum_{i=1}^L P_i \quad (1)$$

where L is the bit length of the binary code P and P_i is the i th bit of P . Ideally, PUF codes should have an equal probability of digits 0 and 1, i.e., a bit uniformity value of 0.5. For both spectral and visual PUFs, histograms of their bit uniformity are plotted in Fig. 4 (C and D), respectively, which show a very narrow distribution centered at 0.505 (for spectra PUFs) and 0.509 (for visual PUFs), thereby validating the good bit uniformity of our silk MP-based PUFs.

HD is commonly used to study the uniqueness and repeatability of PUF codes (16, 41, 42). The HD between two binary codes P and Q is defined as the number of mismatched bits

$$\text{HD}(P, Q) = \sum_{i=1}^L (P_i \neq Q_i) \quad (2)$$

where P and Q are both of length L bits, and P_i and Q_i are the i th bit

of P and Q , respectively. Therefore, HD ranges from 0 to L . If two PUF codes P and Q are identical, $\text{HD}(P, Q) = 0$. For two uncorrelated bit sequences P and Q , $\text{HD}(P, Q) \sim 0.5 L$, because statistically 50% of the bits in P and Q match.

Uniqueness evaluates whether each PUF code can be unambiguously identified. This is characterized by a metric known as intertag HD, defined as the HD between PUF codes obtained from two different tags under the same challenge. For a desirable PUF system, PUF codes obtained from different tags should be uncorrelated and therefore have an intertag HD of $\sim 0.5 L$. The PUF uniqueness is defined as the average of all intertag HDs and computed as below (16)

$$\text{PUF uniqueness} = \frac{2}{K(K-1)} \sum_{x=1}^{K-1} \sum_{y=x+1}^K \frac{\text{HD}(P^x, P^y)}{L} \quad (3)$$

where K is the total number of tags, L is the bit length of each PUF code, and P^x and P^y are the PUF codes obtained from the x th and y th tags under the same challenge, respectively. For 30 different tags (i.e., $K = 30$), there are a total of $30 \times 29/2 = 435$ pairs of comparison, whose HDs were calculated, and the corresponding normalized HDs (i.e., HD/L) were plotted as histograms (shown in yellow bars) in Fig. 4E (for spectral PUFs) and Fig. 4F (for visual PUFs). The histograms of intertag HDs were well-fitted by Gaussian distributions, giving a mean (PUF uniqueness) of 0.497 and an SD of 0.078 for the spectral PUFs, and a mean (PUF uniqueness) of 0.482 and an SD of 0.079 for the visual PUFs. The uniqueness of these PUF codes is better elucidated in Fig. 4G (for spectral PUFs) and Fig. 4H (for visual PUFs), where the (x, y) position displays the $\text{HD}(P^x, P^y)/L$. Good PUF uniqueness is indicated by the nondiagonal elements having colors that correspond to intertag HDs of ~ 0.5 . The clear color contrast between the diagonal and the nondiagonal elements also highlights the uniqueness of the PUF codes.

Repeatability assesses whether the PUF codes obtained from the same tag are reproducible across different measurements. This is characterized by a metric known as intratag HD, which is defined as the HD between PUF codes obtained from the same tag under the same challenge across different measurements. For ideal PUFs, the intratag HD should be 0. To evaluate the PUF repeatability, each silk tag was read by the Raman spectrometer or the pocket microscope twice, producing two PUF codes from the two readouts under the same challenge. The PUF repeatability, defined as the average of all intratag HDs, is computed as below (16)

$$\text{PUF repeatability} = \frac{1}{K} \sum_{x=1}^K \frac{\text{HD}(P^x, R^x)}{L} \quad (4)$$

where K is the total number of tags, L is the bit length of each PUF code, and P^x and R^x are the first (original) and second (repeated) PUF code obtained from the x th tag under the same challenge, respectively. For 30 different tags, all the intratag HDs were calculated and their corresponding normalized HDs were plotted as histograms (shown in blue bars) in Fig. 4E (for spectral PUFs) and Fig. 4F (for visual PUFs). Histograms of the intratag HDs were again fitted by Gaussian distributions, reporting a mean (PUF repeatability) of 0.079 and an SD of 0.024 for the spectral PUFs, and a mean (PUF repeatability) of 0.026 and an SD of 0.028 for the visual PUFs. The repeatability of these PUF codes is better

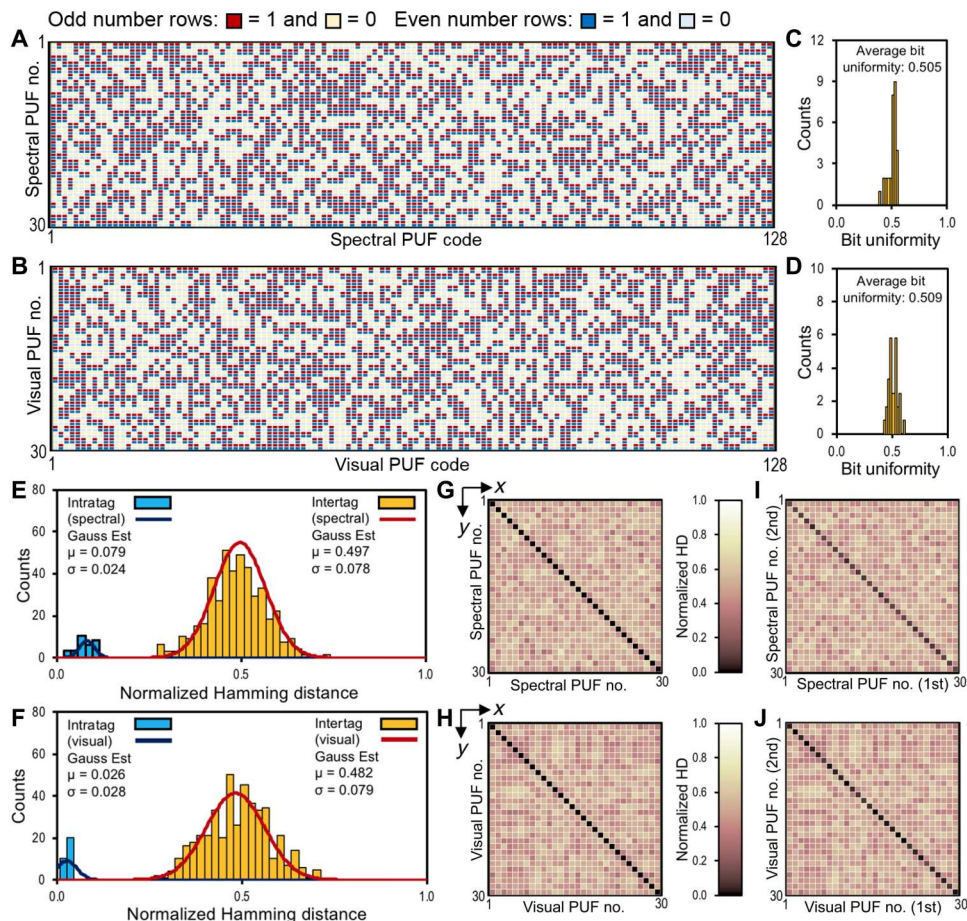


Fig. 4. Evaluation of bit uniformity, uniqueness, and repeatability of the silk MP-based PUFs. (A and B) PUF codes that are repeatedly generated from (A) 30 spectral tags and (B) 30 visual tags under the same challenge. For each tag in (A) and (B), its PUF codes are displayed in two rows with the top and bottom row representing the PUF code obtained from the first (original) and second (repeated) measurement. (C and D) Histograms of the bit uniformity of (C) 30 spectra PUFs and (D) 30 visual PUFs. (E and F) Histograms of intratag HDs and intertag HDs for (E) 30 spectra PUFs and (F) 30 visual tags, along with their Gaussian fitting results. (G and H) Pairwise comparisons among the PUF codes obtained from (G) 30 spectral tags and (H) 30 visual tags. Good PUF uniqueness is indicated by the nondiagonal elements in (G) and (H) having colors that correspond to intertag HDs of ~0.5. (I and J) Pairwise comparisons among the PUF codes obtained from (I) 30 spectral tags and (J) 30 visual tags across two measurements. Good PUF repeatability is indicated by the diagonal elements in (I) and (J) having colors that correspond to intratag HDs of ~0.

elucidated in Fig. 4I (for spectral PUFs) and Fig. 4J (for visual PUFs), where the (x,y) position displays the HD(P^x, R^y)/L. Good

PUF reproducibility is clearly seen by the diagonal elements having colors that correspond to intra-PUF HDs of ~0. The clear color contrast between the diagonal and nondiagonal elements also corroborates that each silk tag can be repeatedly authenticated while retaining its uniqueness.

Last, randomness ensures that each PUF code is a stochastic sequence and cannot be predicted without measuring the actual PUF (i.e., the silk MP's tag). Here, we evaluate the randomness of the PUF codes extracted from our silk tags using a statistical test suite developed by the National Institute of Standards and Technology (NIST) for assessing random number generators for cryptographic applications (43). The 128-bit PUF codes were evaluated using eight tests from the NIST test suite. Each of the eight NIST tests returns a *P* value for each input PUF code, which is considered as random with 99% confidence if its corresponding *P* value ≥ 0.01 . In particular, each of the 30 spectral tags were challenged by 10 random sequences, generating 300 PUF codes (fig. S3A), which were then submitted to the NIST test suite for assessment. For each of the eight tests, Table 1 reports the average *P* value for all the 300 spectral

Table 1. Results of the NIST randomness tests on 300 codes generated from 30 spectral PUFs.

Statistical test	<i>P</i> value	Accuracy	Result
Frequency	0.4657	294/300	Pass
Runs	0.5067	298/300	Pass
Longest runs	0.4791	300/300	Pass
Serial	0.5148	295/300	Pass
	0.4899	295/300	
Approximate entropy	0.4859	295/300	Pass
Cumulative sums	0.4999	298/300	Pass
	0.5076	300/300	

PUF codes along with the pass rate (proportion of PUF codes that pass the corresponding test). The PUF codes are considered to have desirable randomness if the pass rate > 95% (or equivalently >285/300) for each of the eight tests. As shown in Table 1, the spectral PUF codes successfully passed all the randomness tests. The same randomness tests were also performed on 300 codes from the visual PUFs (fig. S3B), and the results of which are summarized in Table 2. Together, we verified the randomness/unpredictability of our silk MP-based PUFs.

Stability of silk MP-based PUFs against environmental factors

Although amorphous silk (i.e., silk molecules in random coils dominated conformations) is susceptible to a few environmental factors such as humidity and temperature, highly crystalline silk (i.e., silk molecules folded in highly ordered structures including but not limited to β sheets, β turns, and α helix) is considered environmentally stable (30). As all the silk MPs used to make the PUF tags are composed of highly ordered silk obtained through either templated crystallization or water annealing for a prolonged time to reach maximum crystallinity, we believe that silk MP-based PUF tags are stable against all environmental factors that might occur during seed storage and transportation over a long period of time. This claim is supported by the repeatability data presented in Fig. 4 where the second measurements of all PUF tags were conducted after storing the tagged seeds for 3 months at room temperature and ambient humidity [i.e., 23°C and 25 to 40% relative humidity (RH)]. Furthermore, we conducted stability and repeatability evaluation of the silk MPs tags stored under extreme humidity (75% RH) and extreme temperature (50°C) for 7 days (figs. S4 to S7). As shown in figs. S4 and S5, spectral tags stored at elevated humidity (75% RH) alone and a combination of elevated temperature and humidity (50°C and 75% RH) show almost identical Raman spectra before and after being stored at corresponding conditions for 7 days, corroborating that neither humidity nor temperature within the feasible range of seed storage conditions has an effect on silk conformation and repeatability of the spectral tags, due to the highly crystalline nature of silk MPs. Similarly, visual tags were not affected by storage at high temperature and humidity (50°C and 75% RH) as the labels showed no observable changes before and after storage and their PUF codes were repeatedly verified over time (figs. S6 and S7).

The biodegradable nature of silk fibroin also does not indicate reduced reliability or increased instability of the silk MPs tag. It has been widely reported in the literature that silk can be degraded by certain proteolytic enzymes (e.g., protease XIV and α -chymotrypsin), soil microbes and in marine environment, and the degradation rates vary from days to years depending on the crystallinity of silk (44, 45). As such, silk is considered as a biodegradable material, which we believe is an advantage as compared to nonbiodegradable materials such as gold nanoparticles and certain plastics that have been used in making PUFs before (17). However, those factors that can degrade silk (i.e., enzymes produced by microbes) do not play a role in materials degradation during normal seed storage and transportation, which typically involve cool, dark, and dry conditions.

DISCUSSION

To summarize, we developed a cryptographic protocol for seed authentication using biopolymer-based PUF tags that can be conformably fabricated on a variety of seeds. Silk MPs of variant polymorphs were fabricated through templated crystallization of silk on different peptide seeds and spray drying of silk followed by water annealing, which serve as the building blocks of our PUF tags. By simply drop casting a mixture of variant silk MPs and amorphous silk on a seed surface, a tamper-evident PUF tag seamlessly formed on the seeds, where the unclonability comes from the stochastic assembly of spectrally distinct silk MPs in the tag. PUF codes of 128 bits were generated on the basis of the intrinsic variations in the Raman spectrum features across different areas of the silk tag. The encoding capability of our silk MP-based PUF can be easily scaled by adjusting the challenge length. Alternatively, addition of colored salts (e.g., FeCl_3) to the silk MPs suspension enables fabrication of a visual PUF whose intrinsic entropy comes from the random distribution of colored silk-iron MPs in the tag. These visual PUFs can be conveniently read by a portable, inexpensive microscope, and then processed for computing the PUF responses. Uniqueness, readout reproducibility, and randomness of the silk MP-based PUFs were also verified by performing standard statistical analyses. These results further guaranteed the robustness of our silk MP-based tags as PUF devices, thus highlighting their applicability as anticounterfeiting labels in real-life scenarios.

For practical applications, we envision that the proportion of seeds being labeled with PUF tags will vary depending on seed type, seed value, and the number of seeds sold in a batch. For high-end products like a special breed of tulip bulbs, one may choose to label each bulb with a unique PUF tag, while for seeds sold in large volumes such as rice seeds, labeling a small portion of seeds randomly picked from a whole batch (also known as the “golden seeds”) should be sufficient for authentication of the entire bag of seeds. There does exist the possibility of swapping golden seeds from one package to another, which is actually one of the common ways of seed counterfeiting (i.e., mixing low-yield, fake seeds with high-quality, authentic seeds). To combat such efforts, our PUF-based authentication of golden seeds can be combined with other established anticounterfeiting technologies, such as tamper-proof packaging and authentication of general, unlabeled seeds through phenotype-based analysis (46), which may not be as accurate as the PUF authentication but provides fast screening of large amounts of seeds at a time.

Table 2. Results of the NIST randomness tests on 300 codes generated from 30 visual PUFs.

Statistical test	P value	Accuracy	Result
Frequency	0.4860	297/300	Pass
Runs	0.5121	296/300	Pass
Longest runs	0.5126	297/300	Pass
Serial	0.5115	296/300	Pass
	0.4748	295/300	
Approximate entropy	0.5087	297/300	Pass
Cumulative sums	0.5420	298/300	Pass
	0.5455	299/300	

When it comes to scanning of the spectral PUF tags, admittedly, most Raman spectrometers are not readily accessible to farmers and general customers with the currently available technology. However, the field of portable Raman for agricultural applications is rapidly advancing, adding merits of miniaturization, lower costs, and shorter spectrum acquisition time (47–49). As an example, handheld Raman spectrometers were recently developed for nondestructive monitoring of plant stresses in the field (50–52). As for verification of the visual PUF tags, the pocket microscope used in this study currently costs less than 23 USD, is battery-powered, and weighs less than 230 g. With a resolution of 1920×1080 pixels, the pocket microscope can be conveniently connected to a smartphone via its built-in Wi-Fi function so that anyone with a smartphone will be able to scan the visual tags and save the captured tag images in their smartphone or on a cloud service within seconds.

Besides its use on agricultural products, we envision that the proposed biodegradable, nontoxic, and edible PUF tags will also provide a useful tool for authentication of food and medicines. Considering that silk has a U.S. FDA-certified GRAS status for human consumption and silk-based food coatings have already been commercialized, we anticipate little regulatory interference and good consumer acceptance. The use of iron in the visual PUFs would presumably be a concern, particularly when the tags are applied to commodities for direct human consumption (e.g., food and medicines). In those scenarios, food-grade cationic dyes (e.g., anthocyanins—a family of water-soluble pigments found in a variety of food such as blueberry and raspberry) could potentially be used to replace Fe^{3+} , considering that the electrostatic interaction between negatively charged silk MPs and colored cations is the major driving force for their coassembly. Together, we believe that the proposed technology based on silk MP-enabled PUFs provides a highly secure solution for product traceability in the Agri-Food domain, and it can be easily adapted to other commodities for anticounterfeiting and beyond.

MATERIALS AND METHODS

Peptide synthesis

All the peptides used in this study were synthesized by GenScript (Piscataway, NJ), with free N and C termini. In brief, peptides were synthesized using standard fluorenylmethyloxycarbonyl-based solid-phase peptide synthesis and purified by reverse-phase high-performance liquid chromatography to a purity of 95% or higher. All peptides were dissolved in pure Milli-Q water.

Silk fibroin regeneration

Silk fibroin was extracted from *B. mori* cocoons following established protocols (53). Briefly, chopped silk cocoons were degummed in a boiling 0.02 M sodium carbonate solution for 30 min to remove the sericin. The obtained silk fibers were then washed with Milli-Q water for several times followed by overnight drying. The dried silk fibers were dissolved in 9.3 M lithium bromide at 60°C for 4 hours, followed by dialysis against Milli-Q water for 2 days with constant changing of water. The resulting silk fibroin solution was then purified by two centrifugation cycles at 20,000g for 30 min each, yielding a final silk fibroin solution of ~7 wt %. The regenerated silk fibroin solution was then stored at 4°C until use.

Preparation of silk MPs

Preparation of silk MPs #1

Spray drying was performed using a model SD-18A LAB Mini Spray Dryer (Labfreez Instruments, China). Under compressed air from an oil-free air compressor (~100 psi), silk fibroin solution at 2 wt % was atomized through a two-fluid nozzle (0.7 mm diameter). The atomizing air flow was adjusted with a flow meter to reach a typical flow rate of 30 liters/min. The silk fibroin solution was fed to the nozzle by a peristaltic pump with a liquid feed rate of 3.33 ml/min. The inlet air temperature was set at 150° to 155°C and the dry air flow rate was 1000 liters/min, which resulted in the outlet air temperature being 75° to 80°C. Silk MPs collected after spray drying were put in a humidified chamber (with an RH of >90%) and incubated for 24 hours. This process is referred to as the water annealing process (30), which induces formation of silk I structures and renders the water-annealed silk MPs water insoluble.

Preparation of silk MPs #2 to 4

To prepare silk MPs #2, silk fibroin solution at 5 mg/ml (i.e., 0.5 wt %) was well mixed with 5 mg/ml (GCGAGA)₂ at a volume ratio of 1:1. After letting the mixture age for 48 hours, the solution was frozen at –80°C for 12 hours, followed by lyophilization at –105°C and vacuum condition for 2 days with a freeze dryer (Free-Zone, Labconco). The lyophilized silk powders were then ground to finer particles using a mortar and pestle. Preparation of silk MPs #3 and #4 follows the same protocol, except by changing the peptides used in templated crystallization to GAGAGSGAAS and HBSP, respectively.

Preparation of silk MPs suspension for PUF tag fabrication

Each of the four silk MPs was first suspended in water to a concentration of 1 wt %, followed by homogenization of the suspension through tip sonication (Branson SFX 550 Sonifier). Each silk MP suspension was sonicated in an ice bath for 5 min with an amplitude of 30% (165-W output power) and pulse durations of 10 s on time and 10 s off time. Following sonication, the 1 wt % suspensions of four silk MPs were well mixed at a volume ratio of 2:1:1:1 by pipetting up and down. Regenerated silk fibroin solution at 1 wt % was then added to the mixed MP suspension at a volume ratio of 3:7, generating a final suspension made of 0.7 wt % (i.e., 7 mg/ml) silk MPs and 0.3 wt % (i.e., 3 mg/ml) amorphous silk molecules. To fabricate spectral PUF tags on seeds, 5 μl of the final suspension was drop cast on each seed and air-dried.

For visual PUF tags, 100 mM FeCl_3 solution was added to the above silk MPs and amorphous silk suspension at a volume ratio of 1:1, generating a final suspension made of 50 mM FeCl_3 , 0.35 wt % silk MPs, and 0.15 wt % amorphous silk. To fabricate visual PUF tags on seeds, 10 μl of the final suspension was drop cast on each seed and air-dried.

Effects of humidity and temperature on the stability of silk tags

Seeds labeled with both spectral and visual PUF tags were stored for 7 days in (i) a sealed container at room temperature (23°C) with saturated NaCl solution to generate a constant RH of 75% and (ii) a sealed container at 50°C with saturated NaCl solution to generate a constant RH of 75%. Each tag was measured by either Raman spectroscopy or pocket microscope before and after storage at corresponding conditions for 7 days and compared to verify the stability of silk MPs tags against extreme humidity and temperature.

Raman mapping of the silk PUF tag

To allow for a defined readout site in each silk PUF tag, a 3-mm by 3-mm mask with a cross-shaped window (0.6-mm by 0.6-mm square with four arms of 0.2 mm length) was cut from an adhesive tape (3M, 467MP) using a laser cutter. The mask was applied to each silk PUF tag on the seeds before Raman reading.

Raman mapping of a $90 \times 90 \mu\text{m}^2$ area within each silk PUF tag (centered at the origin of the mask window) was performed using a Renishaw Invia reflex Raman confocal microscope. A mapping resolution of 4×4 over the $90 \times 90 \mu\text{m}^2$ area was used throughout the study. All Raman spectra were collected over the Raman shift range of 715.8 to 1813.7 cm^{-1} by using a 785-nm laser (100 mW power), a $100\times$ objective [numerical aperture (NA) = 0.90], and a reflectance grating of 1200 lines/mm. Each Raman spectrum was acquired for a total of 30 s (accumulation of 15 spectra, each collected for 2 s).

Imaging of the silk PUF tag

Images of the visual PUF tags (i.e., silk-Fe tags) were captured by a handheld pocket microscope (T TAKMLY Store, Amazon, USA), which offers a resolution of 1920×1080 pixels that corresponds to a 1080P HD picture quality. The pocket microscope was connected to a smartphone using its built-in Wi-Fi function for saving and exporting the images captured.

Generation of PUF challenges

We used a cryptographically secure pseudo random number generator (PRNG) to generate random PUF challenges used for computing the PUF responses from our silk MP-based tags. Our PRNG takes in a 128-bit seed sequence and then expands it by repeatedly encrypting it using the Advanced Encryption Standard cipher with a fixed key (fig. S8) (54). For each encryption event, a sequence of 128 bits was generated, and the process was repeated 10 times in the case of spectral PUFs (to obtain a PUF challenge of 1280 bits) and 12 times in the case of visual PUFs (to obtain a PUF challenge of 1536 bits). We also did postprocessing of the randomly generated challenge sequences to avoid meaningless comparisons. For example, each challenge block for a visual PUF comprises 12 bits that indicate the indexes of two areas a and b whose intensities (i.e., shades of gray) are to be compared. Thus, we need to ensure that a challenge block does not point to the same area (i.e., $a \neq b$). In cases where such meaningless comparisons (i.e., $a = b$) were found, we flipped the lowest bit that correspond to the index of area b .

Computation of PUF codes

Computation of PUF codes from both the spectral and visual readouts of our silk MP-based tags was implemented in MATLAB R2019b. Evaluation of bit uniformity, uniqueness, and repeatability of the PUF codes was also implemented in MATLAB R2019b, while the NIST randomness tests were implemented in Anaconda with a Python script.

Characterization

SEM imaging

The morphology of silk MPs and the microscopic view of the silk PUF tag on seeds were imaged with a Zeiss Gemini 450 scanning electron microscope (SEM), under an acceleration voltage of 1 kV and a probe current of 80 pA. For imaging individual silk MPs, $10 \mu\text{l}$ of 0.1 wt % silk MP suspension was drop cast on a silicon wafer and left to air dry, followed by imaging of the sample under SEM.

TEM imaging

Negatively stained transmission electron microscopy (TEM) images were captured using a Tecnai G² Spirit TWIN microscope operated at 120 kV. For sample preparation, $5 \mu\text{l}$ of each peptide solution (typically at 0.1 mg/ml) was deposited on a glow-discharged continuous-film carbon-coated copper grid (Electron Microscopy Sciences), wicked off after 2 min, and then stained with $5 \mu\text{l}$ of Nano-W (methylamine tungstate, Nanoprobes Inc.) for 1 min before being wicked off. The grid was then left to dry before imaging.

Dynamic light scattering

Dynamic light scattering measurements were performed on a Zetasizer Pro (Malvern Panalytical) under the noninvasive back scattering mode. Silk MP suspension diluted to 0.1 wt % was measured in a low-volume plastic ultraviolet cuvette (BrandTech BRAND). The laser was at 633 nm, and its power was adjusted automatically for different samples to an optimized range of counts by the built-in autoattenuation capability. Measurement of each sample began after equilibration at 25°C for 60 s and was repeated three times to ensure good data repeatability.

Wide-angle x-ray scattering

WAXS measurements were performed on a SAXSLAB instrument in transmission mode with a Dectris Pilatus3R 300 K detector set at a distance of 109.1 mm from the sample and a Rigaku 002 micro-focus x-ray source producing $\text{Cu K}\alpha_1$ x-rays of wavelength 1.5409 Å. Samples were deposited on a thin mica window (5 to 7 μm thick, Molmex Scientific Inc.) and dried before exposing to x-rays. The thin mica windows were chosen owing to their transparency to x-rays with no characteristic peaks in the scattering range of interest. Each spectrum was collected for 5 min.

Supplementary Materials

This PDF file includes:

Supplementary Text
Figs. S1 to S10
References

[View/request a protocol for this paper from Bio-protocol.](#)

REFERENCES AND NOTES

- W. Hong, Z. Yuan, X. Chen, Structural color materials for optical anticounterfeiting. *Small* **16**, 1907626 (2020).
- M. Ni, W. Luo, D. Wang, Y. Zhang, H. Peng, X. Zhou, X. Xie, Orthogonal reconstruction of upconversion and holographic images for anticounterfeiting based on energy transfer. *ACS Appl. Mater. Interfaces* **13**, 19159–19167 (2021).
- H.-J. Jeon, J. W. Leem, Y. Ji, S. M. Park, J. Park, K.-Y. Kim, S.-W. Kim, Y. L. Kim, Cyber-physical watermarking with inkjet edible bioprinting. *Adv. Funct. Mater.* **32**, 2112479 (2022).
- J. Deng, L. Deng, Z. Guan, J. Tao, G. Li, Z. Li, Z. Li, S. Yu, G. Zheng, Multiplexed anticounterfeiting meta-image displays with single-sized nanostructures. *Nano Lett.* **20**, 1830–1838 (2020).
- S. Shikha, T. Salafi, J. Cheng, Y. Zhang, Versatile design and synthesis of nano-barcodes. *Chem. Soc. Rev.* **46**, 7054–7093 (2017).
- Z. Gao, B. Xu, T. Zhang, Z. Liu, W. Zhang, X. Sun, Y. Liu, X. Wang, Z. Wang, Y. Yan, F. Hu, X. Meng, Y. S. Zhao, Spatially responsive multicolor lanthanide-MOF heterostructures for covert photonic barcodes. *Angew. Chem. Int. Ed. Engl.* **59**, 19060–19064 (2020).
- J. V. Rival, P. Mymoona, R. Vinoth, A. M. V. Mohan, E. S. Shibu, Light-emitting atomically precise nanocluster-based flexible QR codes for anticounterfeiting. *ACS Appl. Mater. Interfaces* **13**, 10583–10593 (2021).
- J. Sun, S. Parajuli, K. Shrestha, J. Park, S. Shrestha, Y. Jung, H. Park, G. R. Koirala, N. Nasir, S. Kim, H. Truong, H. Jang, J. Lee, J. Lee, G. Cho, Printed four key-device units for unified platform of wireless anti-counterfeiting label to bridge in blockchain. *Adv. Mater. Technol.* **7**, 2100969 (2022).

9. T. K. Mackey, G. Nayyar, A review of existing and emerging digital technologies to combat the global trade in fake medicines. *Expert Opin. Drug Saf.* **16**, 587–602 (2017).
10. D. Taylor, RFID in the pharmaceutical industry: Addressing counterfeits with technology. *J. Med. Syst.* **38**, 141 (2014).
11. B. Gassend, D. Clarke, M. Van Dijk, S. Devadas, Silicon physical random functions, in *Proceedings of the 9th ACM Conference on Computer and Communications Security*, 148–160 (2002); <https://dl.acm.org/doi/pdf/10.1145/586110.586132>.
12. R. Pappu, B. Recht, J. Taylor, N. Gershenfeld, Physical one-way functions. *Science* **297**, 2026–2030 (2002).
13. G. E. Suh, S. Devadas, Physical unclonable functions for device authentication and secret key generation, in *2007 44th ACM/IEEE Design Automation Conference (IEEE, 2007)*, pp. 9–14.
14. C. Herder, M.-D. Yu, F. Koushanfar, S. Devadas, Physical unclonable functions and applications: A tutorial. *Proc. IEEE* **102**, 1126–1141 (2014).
15. Y. Gao, S. F. Al-Sarawi, D. Abbott, Physical unclonable functions. *Nat. Electron.* **3**, 81–91 (2020).
16. J. W. Leem, M. S. Kim, S. H. Choi, S.-R. Kim, S.-W. Kim, Y. M. Song, R. J. Young, Y. L. Kim, Edible unclonable functions. *Nat. Commun.* **11**, 328 (2020).
17. Y. Gu, C. He, Y. Zhang, L. Lin, B. D. Thackray, J. Ye, Gap-enhanced Raman tags for physically unclonable anticounterfeiting labels. *Nat. Commun.* **11**, 516 (2020).
18. M. S. Kim, G. J. Lee, J. W. Leem, S. Choi, Y. L. Kim, Y. M. Song, Revisiting silk: A lens-free optical physical unclonable function. *Nat. Commun.* **13**, 247 (2022).
19. R. Arppe, T. J. Sørensen, Physical unclonable functions generated through chemical methods for anti-counterfeiting. *Nat. Rev. Chem.* **1**, 0031 (2017).
20. Y. Fan, C. Zhang, Z. Gao, W. Zhou, Y. Hou, Z. Zhou, J. Yao, Y. S. Zhao, Randomly induced phase transformation in silk protein-based microlaser arrays for anticounterfeiting. *Adv. Mater.* **33**, 2102586 (2021).
21. International Seed Federation, “Illegal seed practices—A threat to farmer livelihoods, food security and sustainable agriculture” (2018); <https://worldseed.org/document/illegal-seed-practices-a-threat-to-farmer-livelihoods-food-security-and-sustainable-agriculture/>.
22. X. de Boef, O. Hasson, B. Pierson, D. Kim, J. Mennel, C. Engle, P. Prabhala, J. Bryce, N. Nemeth, A. Jethani, Counterfeiting in African agriculture inputs—challenges & solutions: Comprehensive findings. *Gates Open Res.* **3**, 250 (2019).
23. World Bank, “Enabling the business of agriculture 2017” (2017); <https://elibrary.worldbank.org/doi/abs/10.1596/978-1-4648-1021-3>.
24. C. Wood, H. Hunga, Fighting back against counterfeit seed. *STFC Food Network+* (2022); www.stfcfoodnetwork.org/blog/fighting-back-against-counterfeit-seed.
25. Access to Seeds Foundation, “Access to Seeds Index 2019 - Eastern and Southern Africa” (2019); www.accessseeds.org/index/eastern-southern-africa/.
26. Y. Guan, J. Wang, Y. Tian, W. Hu, L. Zhu, S. Zhu, J. Hu, The novel approach to enhance seed security: Dual anti-counterfeiting methods applied on tobacco pelleted seeds. *PLOS ONE* **8**, e57274 (2013).
27. S. Yigit, N. S. Hallaj, J. L. Sugarman, L. C. Chong, S. E. Roman, L. M. Abu-Taleb, R. E. Goodman, P. E. Johnson, A. M. Behrens, Toxicological assessment and food allergy of silk fibroin derived from *Bombyx mori* cocoons. *Food Chem. Toxicol.* **151**, 112117 (2021).
28. H. Sun, Y. Cao, D. Kim, B. Marelli, Biomaterials technology for AgroFood resilience. *Adv. Funct. Mater.* **32**, 2201930 (2022).
29. M. Liu, P.-E. Millard, H. Urch, O. Zeyons, D. Findley, R. Konradi, B. Marelli, Microencapsulation of high-content actives using biodegradable silk materials. *Small* **18**, e2201487 (2022).
30. H.-J. Jin, J. Park, V. Karageorgiou, U.-J. Kim, R. Valluzzi, P. Cebe, D. L. Kaplan, Water-stable silk films with reduced β -sheet content. *Adv. Funct. Mater.* **15**, 1241–1247 (2005).
31. Y.-F. Maa, P.-A. Nguyen, T. Sweeney, S. J. Shire, C. C. Hsu, Protein inhalation powders: Spray drying vs spray freeze drying. *Pharm. Res.* **16**, 249–254 (1999).
32. H. Sun, B. Marelli, Polypeptide templating for designer hierarchical materials. *Nat. Commun.* **11**, 351 (2020).
33. T. D. Sutherland, S. Weisman, A. A. Walker, S. T. Mudie, The coiled coil silk of bees, ants, and hornets. *Biopolymers* **97**, 446–454 (2012).
34. W. H. Moore, S. Krimm, Vibrational analysis of peptides, polypeptides, and proteins. II. β -Poly (L-alanine) and β -poly(L-alanyl-glycine). *Biopolymers* **15**, 2465–2483 (1976).
35. P. Monti, P. Taddei, G. Freddi, T. Asakura, M. Tsukada, Raman spectroscopic characterization of *Bombyx mori* silk fibroin: Raman spectrum of silk I. *J. Raman Spectrosc.* **32**, 103–107 (2001).
36. M.-E. Rousseau, T. Lefevre, L. Beaulieu, T. Asakura, M. Pézolet, Study of protein conformation and orientation in silkworm and spider silk fibers using Raman microspectroscopy. *Biomacromolecules* **5**, 2247–2257 (2004).
37. C. Colombo, G. Palumbo, J.-Z. He, R. Pinton, S. Cesco, Review on iron availability in soil: Interaction of Fe minerals, plants, and microbes. *J. Soil. Sediment.* **14**, 538–548 (2014).
38. A. T. Zvinavashe, E. Lim, H. Sun, B. Marelli, A bioinspired approach to engineer seed microenvironment to boost germination and mitigate soil salinity. *Proc. Natl. Acad. Sci.* **116**, 25555–25561 (2019).
39. R. E. W. Rafael C. Gonzalez, *Digital Image Processing* (Pearson, ed. 4, 2017).
40. R. Hartley, A. Zisserman, *Multiple View Geometry in Computer Vision* (Cambridge Univ. Press, 2003).
41. M.-D. Yu, R. Sowell, A. Singh, D. M’Raihi, S. Devadas, Performance metrics and empirical results of a PUF cryptographic key generation ASIC, in *2012 IEEE International Symposium on Hardware-Oriented Security and Trust (IEEE, 2012)*, pp. 108–115.
42. V. Suresh, R. Kumar, M. Anders, H. Kaul, V. De, S. Mathew, A 0.26% BER, 10 28 challenge-response machine-learning resistant strong-PUF in 14nm CMOS featuring stability-aware adversarial challenge selection, in *2020 IEEE Symposium on VLSI Circuits (IEEE, 2020)*, pp. 1–2.
43. L. E. Bassham, A. L. Rukhin, J. Soto, J. R. Nechvatal, M. E. Smid, E. B. Barker, S. D. Leigh, M. Levenson, M. Vangel, D. L. Banks, *A Statistical Test Suite for Random and Pseudorandom Number Generators for Cryptographic Applications* (National Institute of Standards and Technology, 2010).
44. C. Guo, C. Li, D. L. Kaplan, Enzymatic degradation of *Bombyx mori* silk materials: A review. *Biomacromolecules* **21**, 1678–1686 (2020).
45. A. T. Zvinavashe, Z. Barghouti, Y. Cao, H. Sun, D. Kim, M. Liu, E. J. Lim, B. Marelli, Degradation of regenerated silk fibroin in soil and marine environments. *ACS Sustain. Chem. Eng.* **10**, 11088–11097 (2022).
46. J. Colmer, C. M. O’Neill, R. Wells, A. Bostrom, D. Reynolds, D. Websdale, G. Shiralaji, W. Lu, Q. Lou, T. Le Cornu, J. Ball, J. Renema, G. F. Andaluz, R. Benjamins, S. Penfield, J. Zhou, SeedGerm: A cost-effective phenotyping platform for automated seed imaging and machine-learning based phenotypic analysis of crop seed germination. *New Phytol.* **228**, 778–793 (2020).
47. W. S. Sutherland, J. P. Alarie, D. L. Stokes, T. Vo-Dinh, A portable surface-enhanced Raman spectrometer. *Instrum. Sci. Technol.* **22**, 231–239 (1994).
48. A. K. Bandyopadhyay, N. Dilawar, A. Vijayakumar, D. Varandani, D. Singh, A low cost laser-Raman spectrometer. *Bull. Mater. Sci.* **21**, 433–438 (1998).
49. M. A. Young, D. A. Stuart, O. Lyandres, M. R. Glucksberg, R. P. Van Duyne, Surface-enhanced Raman spectroscopy with a laser pointer light source and miniature spectrometer. *Can. J. Chem.* **82**, 1435–1441 (2004).
50. T. T. S. Lew, R. Sarojam, I.-C. Jang, B. S. Park, N. I. Naqvi, M. H. Wong, G. P. Singh, R. J. Ram, O. Shoseyov, K. Saito, N.-H. Chua, M. S. Strano, Species-independent analytical tools for next-generation agriculture. *Nat. Plants* **6**, 1408–1417 (2020).
51. S. Gupta, C. H. Huang, G. P. Singh, B. S. Park, N.-H. Chua, R. J. Ram, Portable Raman leaf-clip sensor for rapid detection of plant stress. *Sci. Rep.* **10**, 20206 (2020).
52. P. J. Chung, G. P. Singh, C.-H. Huang, S. Koyyappurath, J. S. Seo, H.-Z. Mao, P. Diloknawarit, R. J. Ram, R. Sarojam, N.-H. Chua, Rapid detection and quantification of plant innate immunity response using Raman spectroscopy. *Front. Plant Sci.* **12**, 746586 (2021).
53. D. N. Rockwood, R. C. Preda, T. Yücel, X. Wang, M. L. Lovett, D. L. Kaplan, Materials fabrication from *Bombyx mori* silk fibroin. *Nat. Protoc.* **6**, 1612–1631 (2011).
54. M. Dworkin, E. Barker, J. Nechvatal, J. Foti, L. Bassham, E. Roback, J. Dray, *Advanced Encryption Standard (AES)* (National Institute of Standards and Technology, 2001); <https://nvlpubs.nist.gov/nistpubs/FIPS/NIST.FIPS.197.pdf>.
55. D. Duvauchelle, “Understanding Pure Live Seed (PLS), Technical Note - PLANT MATERIALS - 03” (Hoolehua, Hawaii, 2021); www.nrcs.usda.gov/plantmaterials/hipmctn13770.pdf.
56. M. J. Houck, “Understanding Seeding Rates, Recommended Planting Rates, and Pure Live Seed (PLS), Plant Materials Technical Note No. 11” (Alexandria, Louisiana, 2009); www.nrcs.usda.gov/plantmaterials/lapmctn9045.pdf.
57. R. K. Rai, V. P. Singh, A. Upadhyay, Chapter 17—Soil analysis, in *Planning and Evaluation of Irrigation Projects*, R. K. Rai, V. P. Singh, A. Upadhyay, Eds. (Academic Press, 2017), pp. 505–523.
58. B. G. Frushour, P. C. Painter, J. L. Koenig, Vibrational spectra of polypeptides. *J. Macromol. Sci. Macromol. Chem.* **15**, 29–115 (1976).
59. A. Sakamoto, M. Tasumi, Symmetry of the benzene ring and its normal vibrations: The “breathing” mode is not always a normal vibration of a benzene ring. *J. Raman Spectrosc.* **52**, 2282–2291 (2021).
60. S. Contorno, R. E. Darienzo, R. Tannenbaum, Evaluation of aromatic amino acids as potential biomarkers in breast cancer by Raman spectroscopy analysis. *Sci. Rep.* **11**, 1698 (2021).
61. S. Krimm, J. Bandekar, Vibrational spectroscopy and conformation of peptides, polypeptides, and proteins. *Adv. Protein Chem.* **38**, 181–364 (1986).

Acknowledgments: We acknowledge the Materials Research Laboratory (MRL) and MIT.nano for access to the characterization instruments, J. Li (MIT) for access to the spray dryer, and M. Liu (MIT) for help with spray drying. **Funding:** This work was partially supported by the Office of

Naval Research (awards N000142112402 and N000141912317) and the NSF (award CMMI-1752172). S.M. was funded partly by Analog Devices Inc. and partly by an MIT EECS Mathworks Fellowship. B.M. acknowledges a Paul M. Cook Career Development Professorship and a Singapore Research Professorship. **Author contributions:** Conceptualization: H.S., S.M., A.P.C., and B.M. Methodology: H.S., S.M., A.P.C., and B.M. Investigation: H.S. and S.M. Visualization: H.S. and S.M. Supervision: A.P.C. and B.M. Writing—original draft: H.S., S.M., and B.M. Writing—review and editing: H.S., S.M., A.P.C., and B.M. **Competing interests:** H.S., S.M., A.P.C., and B.M. are inventors on a patent application (U.S. provisional patent application no. 63/377,156; MBHB ref. no.: 22-1158-US-PRO) filed by Massachusetts Institute of Technology on 26 September 2022 that covers the technology reported in this manuscript. A.P.C. serves on the Board of Analog Devices. B.M. is a cofounder of Mori Inc. The use of silk fibroin as a functional seed coating is

protected by multiple IP positions where B.M. is listed as a coinventor. The authors declare that they have no other competing interests. **Data and materials availability:** All data needed to evaluate the conclusions in the paper are present in the paper and/or the Supplementary Materials. All the codes used in this paper were deposited in Zenodo and can be accessed through <https://zenodo.org/record/7546000> or DOI: 10.5281/zenodo.7546000.

Submitted 5 October 2022

Accepted 17 February 2023

Published 22 March 2023

10.1126/sciadv.adf1978